

# Spectrally Programmable Optical Frequency Comb Generation

Hudi Liu,<sup>§</sup> Yuhan Du,<sup>§</sup> Xingfeng Li, Xingchen Ji,\* and Yikai Su\*

Cite This: *ACS Photonics* 2024, 11, 5195–5204


Read Online

ACCESS |

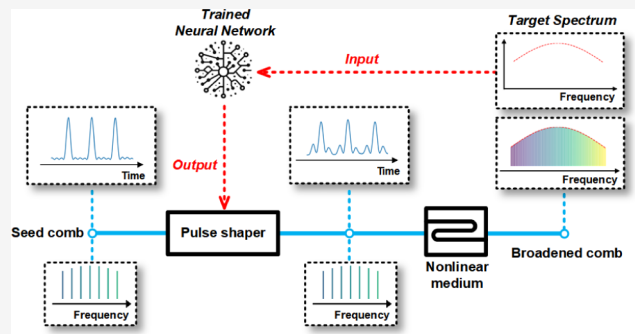
Metrics &amp; More

Article Recommendations

Supporting Information

**ABSTRACT:** Optical frequency combs (OFCs) are critical components in several fields, such as optical communications, microwave photonics, ranging, atomic clocks, and photonic neural networks, which meet diverse application requirements through precise spectral manipulations. Conventional OFC spectral manipulation methods use Fourier transform pulse shapers for postprocessing. However, they face constraints in terms of spectral resolution and operational bandwidth. In this study, a deep-learning-assisted approach is introduced to enable efficient spectral shaping of OFCs through nonlinear broadening, achieving broader spectral shaping by controlling a narrower-bandwidth seed comb. By training a convolutional neural network, we model complex nonlinear interactions within a highly nonlinear fiber to predict and control the spectral output of a broadened comb. Experimental validation confirms the system's ability to generate, with high precision, diverse spectral shapes such as Gaussian, parabolic, Cauchy, Laplace, and Gaussian mixture models within seconds, with a relative error of  $10^{-1}$ – $10^{-2}$ . Our study presents a flexible, rapid, and efficient method for the spectral shaping of OFCs using deep learning, marking a substantial advancement in the programmability and utility of OFC technologies.

**KEYWORDS:** optical frequency comb, spectral shaping, nonlinear optics, deep neural networks, AI for photonics



## INTRODUCTION

An optical frequency comb (OFC) is a coherent light source, which is represented as a series of discrete and equally spaced spectral lines.<sup>1</sup> OFCs have been widely used in many fields, such as optical communication, microwave photonics, ranging, spectroscopy, atomic clocks, and photonic neural networks.<sup>2–6</sup> The versatility of OFCs underscores the significance of precisely controlling their spectral properties to fully exploit their potential for advanced photonic applications. For example, in microwave photonics, the spectral envelope of an OFC can be mapped to the tap coefficients, thus enabling the creation of reconfigurable microwave photonic filters, where different spectral shapes of OFCs can implement various filter functionalities.<sup>7</sup> Similarly, the spectral shaping of OFCs serves as a key technology to encode the weights on the OFC spectrum, facilitating the realization of photonic convolution kernels in photonic neural networks.<sup>3,8</sup> Different spectral shapes of OFCs such as Gaussian, Laplace, and Gaussian mixture model (GMM) can implement neural network capabilities such as noise reduction, blurring, edge extraction, and feature extraction.

The conventional approach for shaping OFCs uses Fourier transform pulse shaper (FTPS) after the comb generation.<sup>3,9,10</sup> An FTPS typically uses gratings to disperse different frequency components, which are then spatially mapped, enabling line-by-line shaping of the OFC spectrum.<sup>11,12</sup> Although the FTPS is a powerful tool for spectral shaping, aligning its operational

bandwidth with the spectral bandwidth of the OFC for effective shaping remains challenging. In addition, for applications that require spectral resolutions  $<10$  GHz, the spectral shaping method based on the FTPS is required to make trade-offs between accuracy, bandwidth, and loss.<sup>13</sup>

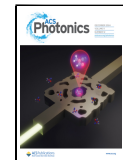
In addition to using FTPS for postprocessing, shaping an OFC during the generation stage provides a promising alternative strategy. Kerr combs, known for their broad spectral bandwidths, allow the generation of microcombs with different soliton states by controlling the structure of the microresonators.<sup>14–18</sup> However, Kerr combs lack spectral tunability as their spectral characteristics are almost fixed, making them less suitable for applications requiring flexible spectral control. Mode-locked lasers offer a more established method, with tunability achieved through temperature adjustments, but they are constrained by their repetition frequencies and tuning ranges, typically spanning hundreds of megahertz to a few gigahertz.<sup>19,20</sup> Electro-optic OFCs (EO-OFCs) stand out for their flexibility, enabling independent control over central wavelengths and repetition frequencies through intensity and

Received: July 30, 2024

Revised: October 29, 2024

Accepted: October 30, 2024

Published: November 12, 2024



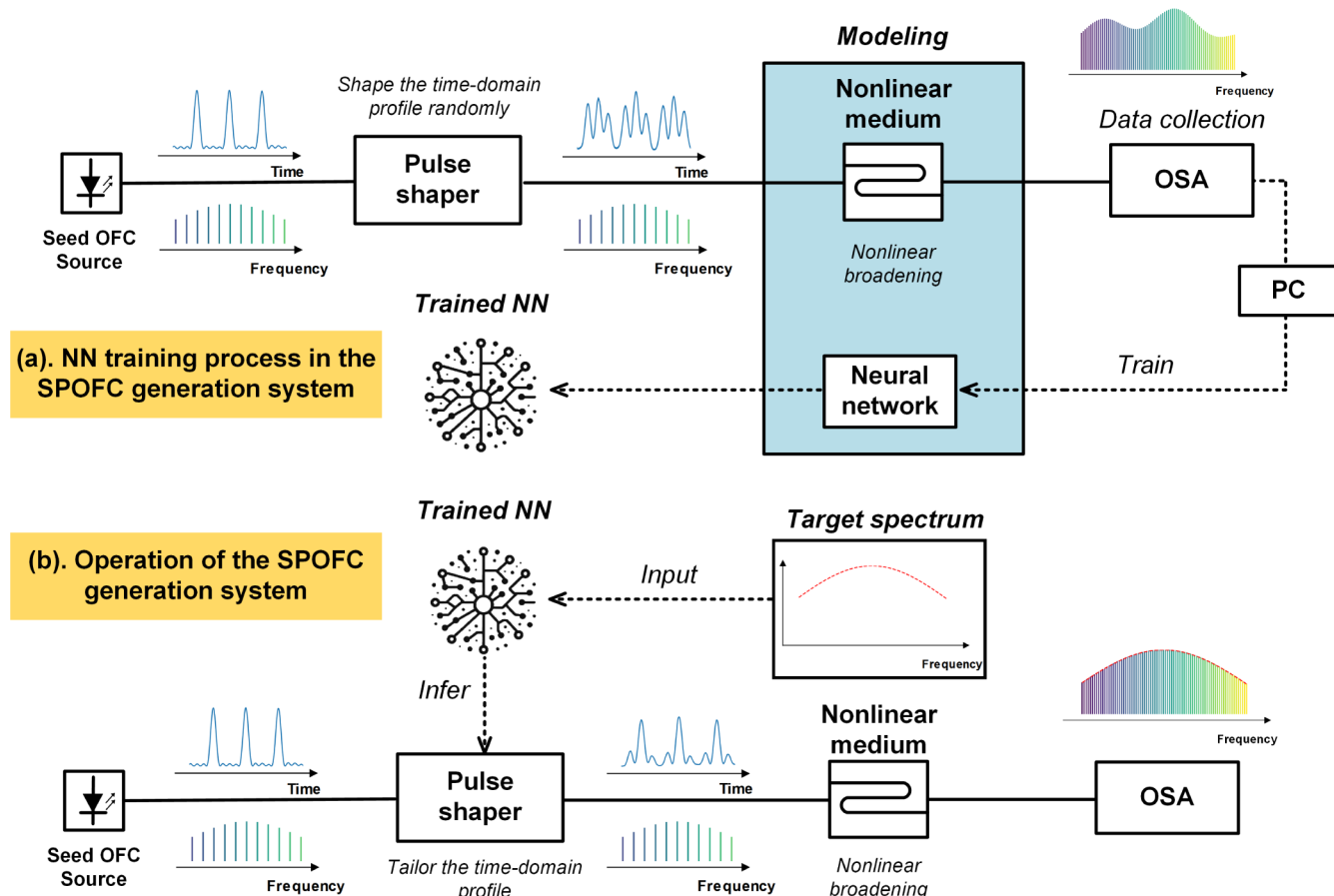


**Figure 1.** Nonlinear spectral shaping process based on a neural network. (a) Neural network (NN) training process in the SPOFC generation system. (b) Operation of the SPOFC generation system. PC, personal computer; OSA, optical spectrum analyzer.

phase modulations. However, EO-OFCs encounter bandwidth limitations and typically require cascade modulators or nonlinear processes for spectral broadening.<sup>21–23</sup> To date, developing a flexible and high-speed spectral shaping scheme for broadband OFCs remains challenging.

Here, we propose a spectrally programmable OFC (SPOFC) generation scheme based on deep learning techniques. We introduce a nonlinear process to the EO-OFC for comb broadening. The spectral envelope of a broadened comb can be affected by modifying the temporal profile of the seed EO-OFC. Given the intricate nonlinear nature of the EO-OFC-broadening process, we trained a convolutional neural network (CNN) model to represent the complex inverse process of the nonlinear spectral broadening of OFCs in a highly nonlinear fiber (HNLF). The CNN was finely tuned to predict the phase feature parameters of the seed OFC to ensure tailored shaping of the broadened spectrum. Compared with using FTPS to shape the OFC spectrum directly, our scheme needs to control only one-tenth of the bandwidth to shape the broadened OFC accurately in the experiment, without introducing additional loss elements. In addition, the neural-network-based approach significantly reduces inference time compared to other previously reported computational methods, such as evolutionary strategies and genetic algorithms.<sup>22,24,25</sup> Therefore, our scheme allows second-level switching between different OFC spectra, significantly outperforming the minute-to-hour computation times required by traditional iterative solutions.

## RESULTS

### Nonlinear Spectral Envelope Shaping with Neural Network.

Using nonlinear effects in optical fibers or waveguides is a common strategy for broadening the OFC bandwidth.<sup>26</sup> In this study, we controlled the nonlinear broadening process of seed OFCs to shape the spectra of the broadened OFCs. Spectral expansion was driven by nonlinear effects induced by high optical intensities and long interaction lengths within the nonlinear medium. These nonlinear effects intricately shape the comb spectrum, and the nonlinear progress is influenced by parameters, such as nonlinear coefficients, dispersion, and input power. To analyze these phenomena, the generalized nonlinear Schrödinger equation provides a theoretical framework for modeling the propagation of electromagnetic waves in dispersive nonlinear media.<sup>27</sup>

$$\frac{\partial A}{\partial z} + \frac{\alpha}{2} A - \sum_{n=k}^{+\infty} \frac{i^{n+1} \beta_n}{n!} \frac{\partial^n A}{\partial t^n} = i\gamma |A|^2 A \quad (1)$$

where  $A(z, T)$  is the slowly varying amplitude,  $z$  is the propagation distance,  $\beta_n$  is the  $n$ th-order dispersion coefficient,  $\alpha$  is the loss coefficient, and  $\gamma$  is the nonlinear coefficient.

The key to effectively modifying the OFC spectrum through nonlinear effects is the accurate calculation of the pulse shape entering the nonlinear medium. While the NLSE provides a structured approach to predict comb evolution, tuning the spectrum by adjusting parameters, such as dispersion or input power, becomes challenging when higher-order nonlinearities

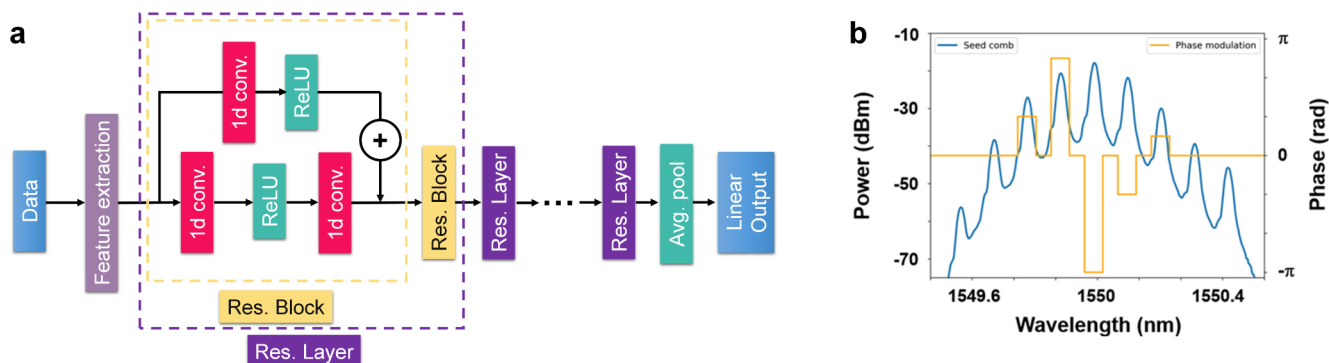


**Figure 2.** 1D-ResNet model design. (a) 1D-ResNet model structure. 1D conv., one-dimensional convolutional layer; ReLU, a kind of nonlinear activation function; Res. Block, residual blocks; Avg. pool, average pool. (b) Schematic diagram of the transfer function of the pulse shaper. The blue curve is the spectrum of the seed comb in the experiment, and the yellow line is one of the phase shifts applied by the pulse shaper to the comb teeth at different frequencies.

are involved. Nonlinear effects such as self-phase modulation, Raman scattering, and four-wave mixing interact in complicated ways, making direct parameter tuning insufficient for precise spectral control. As nonlinear order increases, predicting their combined impacts on the comb spectrum becomes increasingly difficult. Methods for controllable spectrum broadening include the inverse split-step Fourier method coupled with optimization algorithms and specific spectrum configurations using iterative adaptive algorithms.<sup>22,25</sup> However, the reliability of pulse-shaping function computations is largely dependent on the assumptions of the inherent properties of the pulse and the characteristics of the nonlinear medium. Using adaptive algorithms, such as evolutionary strategies, for adaptive pulse shaping increases the computational complexity considerably, resulting in extended optimization periods and time. It is worth noting that the scalability and accuracy of these approaches are limited by the complexity of the required spectrum.

In order to overcome these limitations, we proposed an approach to model the inverse process of OFC broadening in nonlinear media using neural networks. As shown in eq 1, the influence of the high-order nonlinearity on the broadening process is paramount. Compared with conventional numerical methods, the neural-network-based approach excels in adapting to high-order nonlinear effects owing to its proficiency in learning from complex data patterns and flexibility in model configuration. By training on extensive datasets that capture the nuances of nonlinear interactions, neural networks can accurately predict the OFC evolution in nonlinear media, seamlessly integrating high-order nonlinear dynamics without explicit mathematical formulations. Furthermore, in practical experimental settings, factors such as manufacturing imperfections, environmental fluctuations, and noise from components such as the EDFA can significantly affect the comb spectrum. Conventional NLSE-based models struggle to account for these variables, whereas neural networks can capture such variability through experimental data and offer more reliable predictions for spectral shaping.

As depicted in Figure 1, neural networks can complete the modeling process precisely without prior knowledge of the specifics of a nonlinear medium through data-driven training. After the desired input pulse shape for the nonlinear medium is determined based on the target spectrum, the pulse shaper modifies the time-domain profile of the seed OFC. The tailored OFC then undergoes nonlinear propagation, generat-

ing a specified broadened spectrum. This neural-network-based approach not only mitigates the potential adverse effects of high-order nonlinearity on spectral shaping but also opens avenues for exploiting these nonlinearities to enhance system performance. Additionally, since we did not provide the model with explicit prior information about experimental parameters, such as the seed comb spectrum or the nonlinear coefficients of the medium, the model demonstrates broader portability. This allows it to be retrained on similar experiments using appropriate datasets without requiring changes to the network architecture.

### Learning the Nonlinear Broadening Process through CNN.

We employed a deep learning method to capture the intricate nonlinear nature of the broadening process and model the complex relationships in OFC pre- and postbroadening. Specifically, we used a one-dimensional residual neural network (1D-ResNet), which was a CNN architecture comprising multiple residual blocks. We chose 1D-CNNs for this task due to their ability to capture local patterns and dependencies in sequential data, particularly for signals and spectra.<sup>28,29</sup> Moreover, 1D-CNNs offer parameter efficiency through weight sharing and an enhanced capacity to learn complex nonlinear relationships using residual connections.<sup>30</sup> These characteristics make 1D-CNN, particularly the 1D-ResNet architecture, a highly suitable choice for understanding the intricate nature of the broadening process. As shown in Figure 2a, 1D-ResNet was constructed using one input layer, followed by several residual blocks and an output layer. This configuration enables the network to undergo extensive training epochs, effectively overcoming the challenges posed by traditional CNNs in learning highly complex nonlinear processes.<sup>31</sup>

For variations in the spectral information distribution across different target spectra, we incorporated a feature extraction layer as the input layer. This layer used the convolution method to increase the channel depth and capture localized features, enhancing the representational capacity of the model. Within the hidden layers, the network contained several residual layers, each comprising two residual blocks. Each residual block is composed of two convolutional layers. The number of residual layers was determined by the dataset size and the required level of hierarchical feature abstraction. Through the sequential application of multiple residual layers and activation functions, a neural network can be used to model the inverse propagation of light pulses in a nonlinear

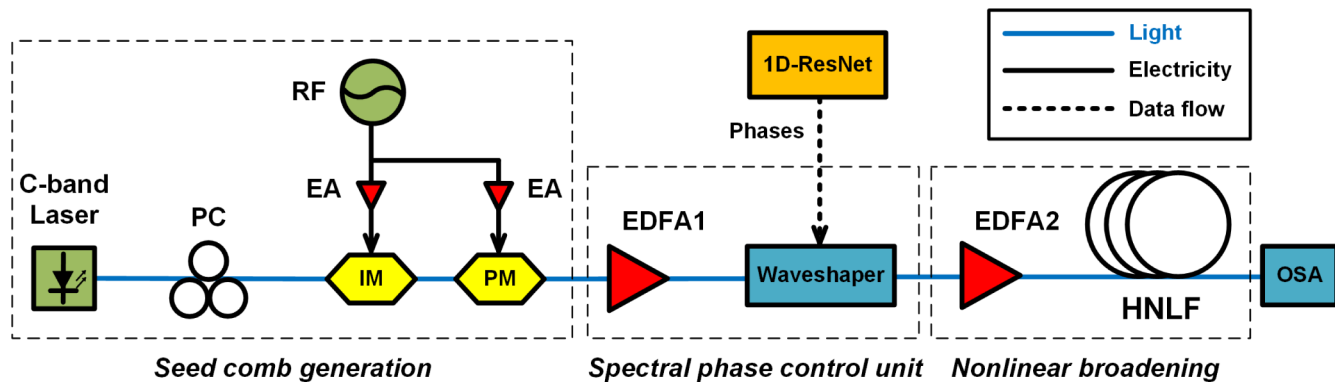


**Figure 3.** Experimental setup of the SPOFC generation system. RF, radio frequency signal generator; EA, electrical amplifier; IM, intensity modulator; PM, phase modulator; EDFA, erbium-doped optical amplifier; HNLF, highly nonlinear fiber; OSA, optical spectrum analyzer.

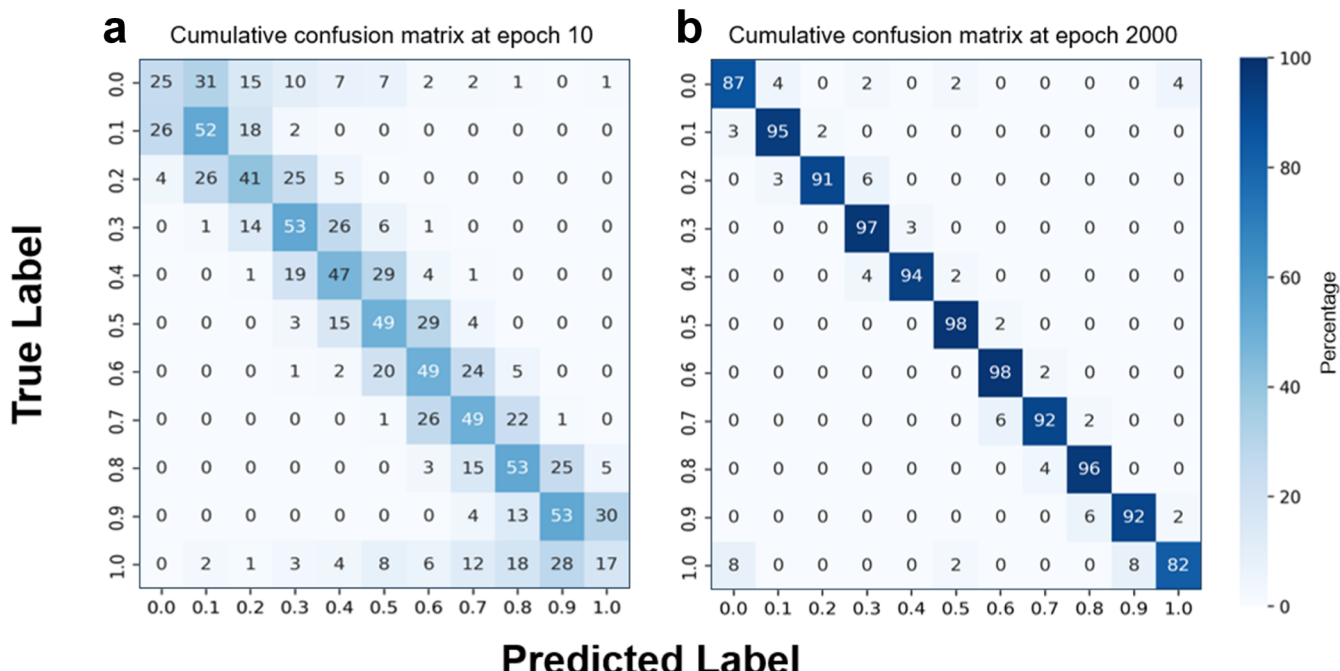


**Figure 4.** Comparison of the cumulative confusion matrices for the model under different loss values. (a) Cumulative confusion matrix when the model loss is 0.017 after 10 learning epochs. (b) Cumulative confusion matrix when the model loss is 0.006 after 2000 learning epochs.

medium. We applied batch normalization after each convolutional layer to enhance the stability and expedite the convergence of the model.

The output from the 1D-ResNet formed the basis for adjusting the transfer function of the pulse shaper. Typically, the 1D-ResNet infers the time-domain waveform sequence of the target EO-OFC. Considering the limited capabilities of commercial waveshapers, we simplified the requirements of the pulse shaper's performance, allowing it to only shift the phases of the individual comb teeth across different frequencies, rather than simultaneously controlling the intensities. To describe the temporal profile of the seed comb, we introduced five phase features corresponding to the phase adjustments applied to the five central comb lines of the seed comb, as illustrated in Figure 2b. We controlled the phase of five comb lines as a balance between effective spectral shaping and maintaining system simplicity and control accuracy. The output layer contains a fully connected layer to generate a 1D vector comprising the five phase features.

**Setup of the Proof-of-Principle Experiment.** The experimental system consisted of three principal stages: seed comb generation, spectral phase control, and nonlinear broadening, as illustrated in Figure 3. The seed comb, generated through electro-optical modulation, passes through a spectral phase control unit before entering a nonlinear medium, using spectral broadening to achieve the desired spectrum.

For the seed comb, we used an EO-OFC, which was chosen for its flexibility in adjusting the repetition rate and central wavelength in addition to its high coherence and robustness. We used an architecture consisting of an intensity modulator (IM) and phase modulator (PM) cascade because the generation of the seed comb was not confined to a specific spectral profile. These modulators were driven by a sinusoidal radio frequency (RF) signal that generated an EO-OFC with a narrow bandwidth. The repetition frequency was controlled by the sine wave frequency of the RF oscillator, and the central frequency was aligned with the wavelength of the light source. We used a high-precision RF signal generator to ensure RF

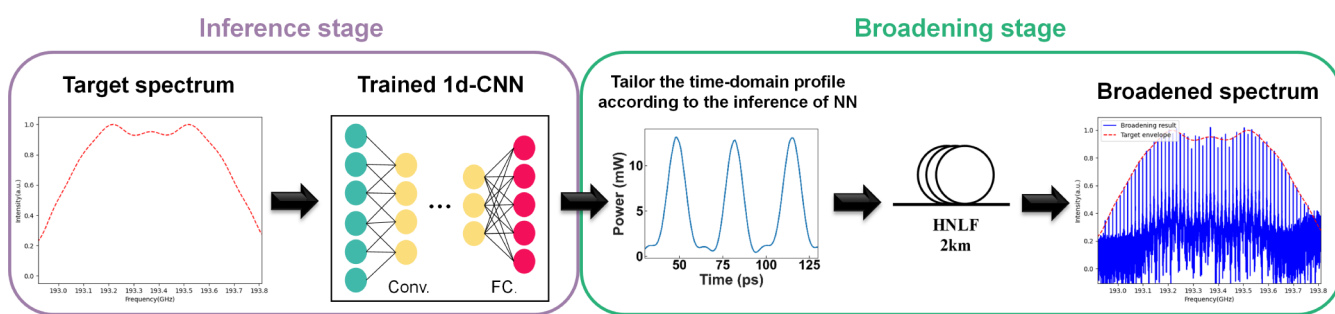


**Figure 5.** Prediction and validation flow of the SPOFC generation system.

signal stability, as the system can tolerate minor fluctuations in the repetition rate, but significant changes will introduce disruptions in the neural network's training process. In the experiment, we set the central wavelength of the light source to 1550 nm and the frequency of the RF signal to 10 GHz. A significant observation is the susceptibility of the IM bias to drift, potentially altering the EO-OFC over time, which could influence subsequent data collection. To compensate for this variability, a bias control circuit was employed to maintain the IM bias point within the quadrature mode, effectively minimizing seed comb fluctuations during data acquisition.

Following the generation of the seed comb, the temporal profile was tailored based on the inferences from the neural network. This tailoring process required adjustment of the phase characteristics of the seed comb, focusing on five key phase features. In practical terms, a liquid-crystal-on-silicon-based spectral shaper (Finisar WaveShaper) was employed to apply the phase shifts to the five comb lines within a range of  $(-\pi, \pi)$ . It is worth noting that although the waveshaper was used in the experiments to modify the phase parameters of the seed comb for the purpose of simplifying the experimental setup, it is actually possible to achieve a similar functionality using a lower cost solution such as a phase shifter array.

To avoid a complex spatial alignment in the nonlinear broadening stage, we used HNLF as the nonlinear medium required for broadening. The seed comb was amplified by an erbium-doped fiber amplifier (EDFA) and then fed into a 2-km HNLF with a zero-dispersion window at 1550 nm and a 0.03 ps/nm<sup>2</sup>-km dispersion slope. An HNLF operating in the normal dispersion region was chosen to prevent adverse effects, such as modulation instability. We optimized the EDFA gain to minimize the noise effect. In addition, we trained the neural network on datasets that included system noise, allowing it to effectively account for this noise during the training process and ensure accurate comb generation in the presence of system noise.

**Experimental Results.** In this study, we established a dataset for the OFC-broadening process based on nonlinear media through the experimental setup in Figure 3. We generated about 10 000 sets of data by randomly applying five phase perturbation values across these comb lines using a pulse shaper, with an optical spectrum analyzer (OSA) capturing the broadened comb spectra at a resolution of 0.02 nm. The dataset comprised of 10 000 data points, and the input power to the HNLF was amplified to 23 dBm by the EDFA2. After training the model on this dataset, we evaluated its performance using the confusion matrix. Since the five outputs have the same range and similar physical significance, we summed the five confusion matrices to form a cumulative confusion matrix. Figure 4 compares the normalized

cumulative confusion matrix of five outputs in different training stages with the real label distribution. With reference to the percentage color bar, it can be seen that the dark blocks are gradually distributed on the diagonal, which means that the output is equal to the label, verifying the effectiveness of the training and the accuracy of the network.

To evaluate the performance of the generation system, we generated a series of target spectra using several common functions and modified their feature parameters to obtain a diverse range of target spectra external to the dataset. As shown in Figure 5, we used a trained 1D-ResNet instrument to infer the five phase feature parameters of the seed comb corresponding to the target spectra. We modulated these parameters on the seed comb and used an HNLF for nonlinear broadening. Throughout the training process, we observed a reduction in the mean squared error (MSE) loss for both the training and validation sets, reaching levels of  $10^{-5}$  and  $10^{-3}$ , respectively. To capture the model at its peak performance, we implemented a checkpoint strategy involving saving the model configuration with the lowest validation loss.

The initial validation involved the generation of Gaussian-shaped spectral envelopes. The formula of the Gaussian function is as follows:

$$f(x) = \alpha e^{-\frac{(x-\mu)^2}{2\sigma^2}} \quad (2)$$

where  $\alpha$  is the default value of 1,  $\mu$  is the default value of 0,  $\sigma$  is the standard deviation, and  $x$  represents the independent variable corresponding to the horizontal axis. OFCs with Gaussian-shaped spectral envelopes have broad applications in photonic neural networks, such as smoothing and denoising image-processing tasks. By modifying the parameter  $\sigma$ , the function can be customized to meet specific requirements. We focused on varying the  $\sigma$  values within the range of 0.1–0.4, incrementing in steps of 0.1, and examined the effects on the attributes of the Gaussian-shaped envelope. We constructed the Gaussian function over the  $x$  domain of  $(-1, +1)$ . We then rescaled the  $x$ -axis to the interval (1546, 1554) while preserving the value of  $f(x)$  corresponding to the Gaussian distribution. By applying this linear transformation, we can map Gaussian functions of different  $\sigma$  onto the spectra of OFCs with a wavelength range of 1546–1554 nm. To compare the performance of different envelope shaping methods, we used the relative error  $\epsilon$  to determine the similarity between the generated and target spectral envelopes in the region of interest (ROI):<sup>32</sup>

$$\epsilon = \frac{\|T - S\|_2}{\|S\|_2} \quad (3)$$

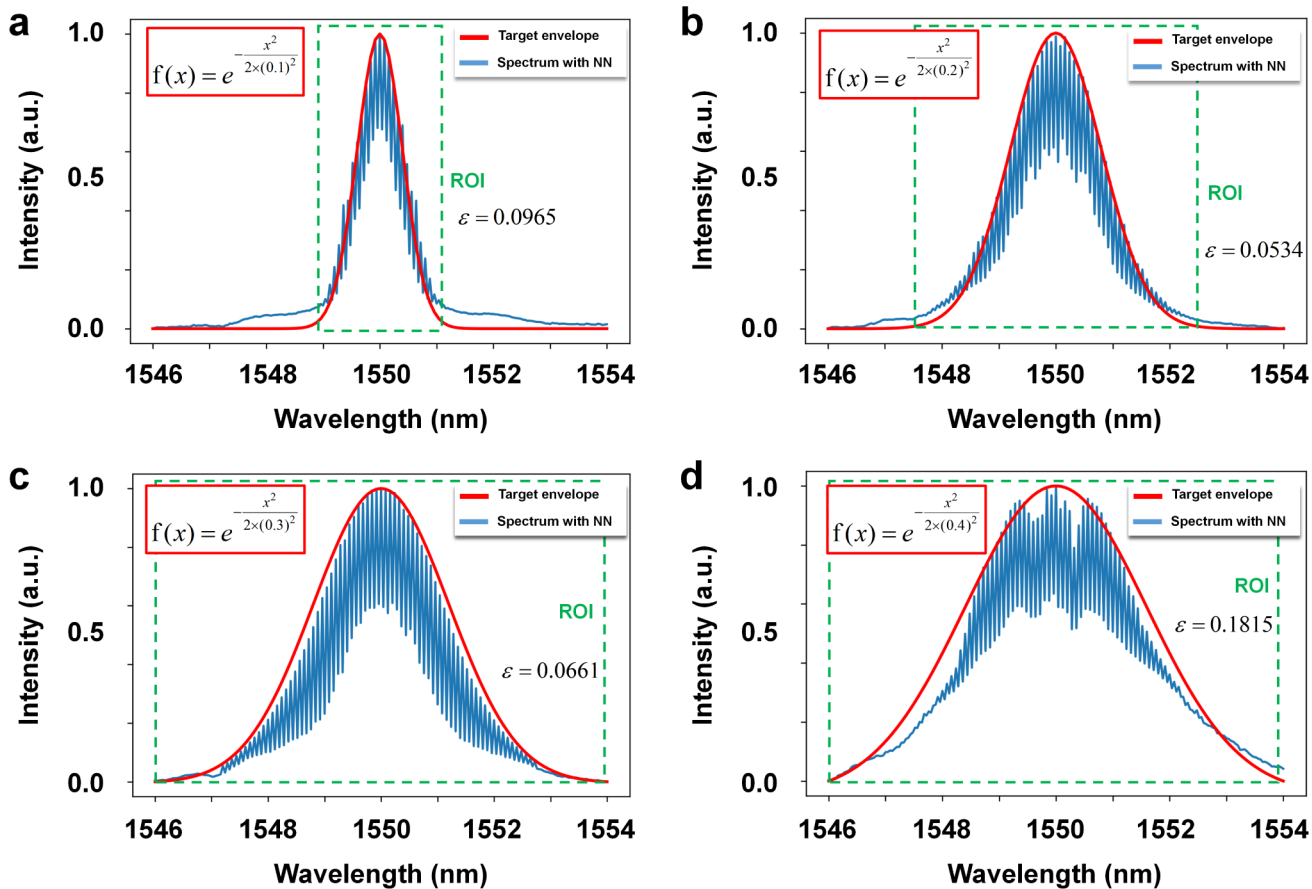


**Figure 6.** Gaussian-shaped OFC generation with 1D-ResNet. (a–d) Different target Gaussian envelopes with characteristic parameters  $\sigma$  of 0.1, 0.2, 0.3, and 0.4. Red curves are target envelopes. Blue curves are the experimental results of the OFCs. The green dashed line box is the region of interest (ROI), defined as the region of the target envelope where the value exceeds 0.01.

where  $T$  is the target spectral envelope and  $S$  is the broadened spectral envelope.

Figure 6a–c demonstrates the effectiveness and superiority of the proposed SPOFC generation system for generating OFCs that closely match the desired Gaussian-shaped envelopes. However, as  $\sigma$  increases to 0.4, Figure 6d shows a progressive expansion in the OFC bandwidth and an increase in the  $\varepsilon$  value. This phenomenon can be attributed to the physical limitations of the experimental setup, such as the nonlinear parameters of the HNLF and the seed comb power entering the HNLF, which restrict the programmable range of the OFC spectrum. The suboptimal performance is due to insufficient nonlinear effects at this power level. The limitation is not related to the neural network's capability, which remains adaptable across varying power conditions. Similarly, the current experimental setup was not optimized to generate a flat-top spectrum, which typically requires higher power levels, such as 30 dBm, to achieve uniform intensity across the spectrum.<sup>33</sup> Further discussion on the programmable range can be found in Section S3 of the Supporting Information.

To further evaluate the versatility and efficacy of the SPOFC generation system, we performed an analysis with alternative parabolic, Cauchy, and Laplace envelope shapes. We modified the characteristic parameters of these functions and normalized them to the range (0, 1) as target envelopes. We also rescaled the  $x$ -axis to the interval (1546, 1554) according to the span of target OFCs in the experiment. The experimental results depicted in Figure 7 illustrate the capability of the SPOFC

generation system to produce OFCs corresponding to diverse target envelopes. The experimentally generated spectra obtained by using the SPOFC generation system exhibited good consistency with the target spectra.

We further verified the programmability of the SPOFC generation system by generating OFCs with envelopes formed by summing multiple Gaussian functions. By changing the values of  $\alpha$ ,  $\mu$ , and  $\sigma$  in eq 2, we obtained different Gaussian functions to form a GMM representing the target envelope. By iteratively fitting the appropriate GMMs, we can achieve spectral shaping at the level of a few comb teeth. As shown in Figure 8, the generated spectra demonstrated high similarity to those of the target envelopes. Although we cannot directly generate a flat-top spectrum using the experimental setup discussed earlier, it is still a feasible method to approximate the flat-top spectrum using the GMM, as shown in Figure 8d. The results demonstrate the ability of the SPOFC generation system to generate complex, multipeaked spectral envelopes with exceptional accuracy, further highlighting its programmability and versatility in shaping OFC spectra for different applications.

In the experiment, we changed the phases of the five central combs of the EO-OFC within a bandwidth of 60 GHz, facilitating control over the spectral shape across an expansive bandwidth of approximately 1000 GHz. Furthermore, as 1D-ResNet inferred the phase characteristic parameters for the target spectra within seconds, the SPOFC generation system

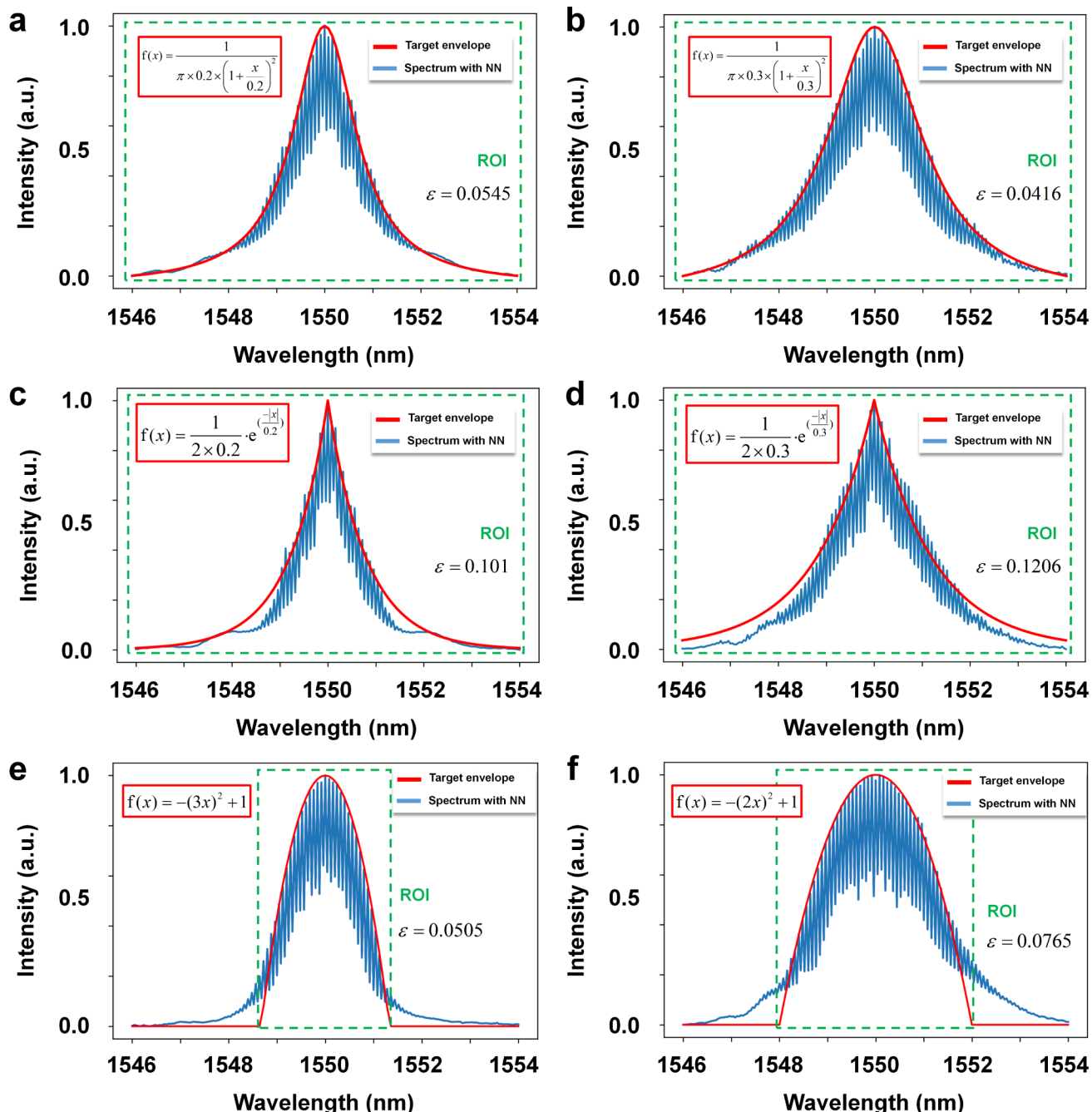


**Figure 7.** SPOFC generation for different common functions. (a,b) Cauchy envelopes whose expression is  $f(x) = 1/[\pi \cdot \sigma \cdot (1 + x/\sigma)^2]$  with different characteristic parameters  $\sigma$  of 0.2 and 0.3. (c,d) Laplace envelopes whose expression is  $f(x) = 1/(2 \cdot \sigma) \cdot \exp(-|x|/\sigma)$  with different characteristic parameters  $\sigma$  of 0.2 and 0.3. (e,f) Parabolic envelopes whose expression is  $f(x) = -(ax)^2 + 1$  with characteristic parameters  $a$  of 3 and 2. The green dashed line box is the ROI, which is defined as the region of the target envelope where the value exceeds 0.01.

achieved second-level switching between the different spectra of the OFCs.

## DISCUSSION

Building on the performance of SPOFC generation systems, the integration of tunable and rapid OFC spectral shaping technologies offers possibilities for real-time adaptive optical computing. For example, photonic convolutional kernels in optical neural networks offer a powerful solution for high-speed, large-scale, and complex data processing tasks with the ability to scale and integrate into different hardware systems, providing a significant advantage over traditional electronics-

based neural networks.<sup>34</sup> The ability of the SPOFC generation system to customize OFC spectral envelopes rapidly means that the characteristics of convolutional kernels can be adapted in real time to meet the demands of different computational tasks. Switching between different envelope shapes such as Gaussian, parabolic, and Cauchy allows for the adjustment of the kernel's frequency response and, consequently, the characteristics of the optical neural network.

In applications such as reconfigurable microwave photonic filters, the SPOFC system can rapidly adjust the kernels to adapt to changing signal environments or filter out specific interference patterns, enhancing the adaptability and robust-

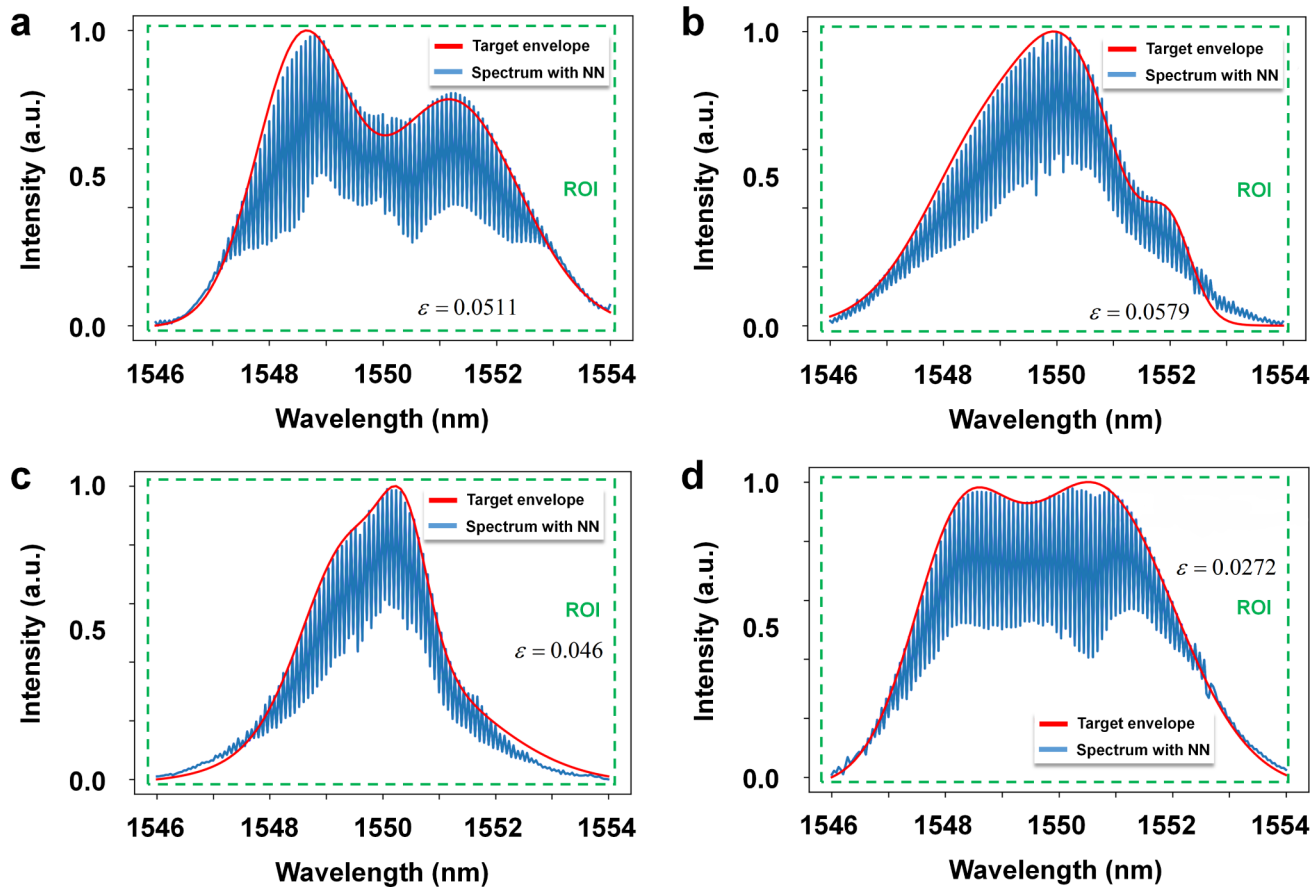


**Figure 8.** SPOFC generation for different Gaussian mixture models. (a) Two Gaussian functions. (b–d) Three Gaussian functions.

ness of communication systems.<sup>7</sup> Similarly, in the context of photonic neural networks, the ability to reprogram the spectral characteristics instantaneously paves the way for adaptive learning and dynamic network reconfiguration, which are critical for real-world deployment, where operating conditions are variable and unpredictable.

## CONCLUSION

We established an SPOFC generation system by using deep learning techniques. Using the nonlinear broadening process within the EO-OFC, we took this stage for comb shaping while preserving the central frequency and repetition rate tunability of the entire system. To address the intricate nonlinear nature of the OFC-broadening process, a 1D-ResNet model was trained to represent the complex inverse process occurring in an HNLF. The 1D-ResNet efficiently inferred the phase feature parameters of the seed OFC within seconds, enabling precise shaping of the broadened OFC spectra with  $\epsilon$  values on the order of  $10^{-1}$  and  $10^{-2}$ . The experimental validation underscores the efficacy of our OFC generation scheme, showing exceptional results across diverse envelopes including Gaussian, parabolic, Cauchy, Laplace, and Gaussian mixture functions with varying feature parameters. Our work demonstrates a flexible, rapid, and efficient method for the spectral shaping of OFCs using deep learning, promising extensive applications across diverse fields reliant on OFCs.

## METHODS

**Detailed Experimental Setup.** Generation of the seed comb was initiated by using a tunable laser source (TLS150D,

Southern Photonics) with a central emission wavelength of 1550 nm. The laser output was directed into an electro-optic modulation system comprising an IM (FTM793EK, Fujitsu) and PM (MPZ-LN-20, iXBLUE). The modulators were driven by a high-precision RF signal generator (APSIN20G, Anapico) operating at a frequency of 10 GHz. This configuration allowed the creation of an EO-OFC with an adjustable repetition rate and wavelength. A bias-control circuit was integrated with the IM to stabilize its operation and counteract potential bias drifts, thereby maintaining the stability of the seed comb. Following the generation of the seed comb, the spectral phase was tailored to achieve the desired broadening results. This was accomplished using a neural-network-driven approach in which phase adjustments were applied to five specific comb lines. The phase control was implemented using a spectral shaper (WaveShaper 1000s, Finisar Corp.), which applied precise phase shifts within the range of  $(-\pi, +\pi)$ . The broadening of the EO-OFC involved amplifying the comb with an EDFA (EDFA-C-BA27) and subsequently transmitting it through a 2-km HNLF (NL-1550-Zero, YOFC). The HNLF was selected for its zero-dispersion at 1550 nm and low dispersion slope, ensuring effective broadening while mitigating risks, such as modulation instability.

**Neural Network Training.** The dataset collected during the experiment was segmented on a scale of 0.1, resulting in 8500 samples for training and 1000 samples for validation. The CNN architecture consisted of an input layer, eight residual blocks, and an output layer with five nodes. The number of nodes in the input and output layers was determined by the bandwidth of the experimentally measured spectrum, the

resolution of the OSA, and the number of phase parameters used to define the time-domain profile of the seed comb. The activation function in the neural network was selected as a rectified linear unit (ReLU) to introduce nonlinearity and improve the learning capacity of the model. To prevent overfitting during the learning process, batch normalization was added to the residual blocks. The Adam optimizer was used to minimize the MSE loss function, and the learning rate was set to  $3 \times 10^{-4}$ . During CNN training, batch learning with a batch size of 100 was used. The CNN was implemented using the PyTorch 1.10.0 Python library in Python version 3.8.9. The experiments were conducted on a desktop computer equipped with an Nvidia RTX 3070 Ti GPU, an AMD Ryzen 7 5800 CPU (8-core), and the Microsoft Windows 11 operating system.

## ASSOCIATED CONTENT

### Data Availability Statement

The datasets and codes used during the current study are available from the corresponding author upon reasonable request.

### Supporting Information

The Supporting Information is available free of charge at <https://pubs.acs.org/doi/10.1021/acsphtronics.4c01422>.

Details about the neural network structure and training, generation of neural inputs, and additional experimental results ([PDF](#))

## AUTHOR INFORMATION

### Corresponding Authors

**Yikai Su** – State Key Laboratory of Advanced Optical Communication Systems and Networks, Department of Electronic Engineering, Shanghai Jiao Tong University, Shanghai 200240, China;  [orcid.org/0000-0002-1526-8187](https://orcid.org/0000-0002-1526-8187); Email: [yikaisu@sjtu.edu.cn](mailto:yikaisu@sjtu.edu.cn)

**Xingchen Ji** – John Hopcroft Center for Computer Science, School of Electronic Information and Electrical Engineering, Shanghai Jiao Tong University, Shanghai 200240, China;  [orcid.org/0000-0002-0284-0818](https://orcid.org/0000-0002-0284-0818); Email: [xingchenji@sjtu.edu.cn](mailto:xingchenji@sjtu.edu.cn)

### Authors

**Hudi Liu** – State Key Laboratory of Advanced Optical Communication Systems and Networks, Department of Electronic Engineering, Shanghai Jiao Tong University, Shanghai 200240, China;  [orcid.org/0009-0002-4038-1963](https://orcid.org/0009-0002-4038-1963)

**Yuhan Du** – State Key Laboratory of Advanced Optical Communication Systems and Networks, Department of Electronic Engineering, Shanghai Jiao Tong University, Shanghai 200240, China

**Xingfeng Li** – State Key Laboratory of Advanced Optical Communication Systems and Networks, Department of Electronic Engineering, Shanghai Jiao Tong University, Shanghai 200240, China

Complete contact information is available at:  
<https://pubs.acs.org/10.1021/acsphtronics.4c01422>

### Author Contributions

<sup>§</sup>H.L. and Y.D. contributed equally to the article. H.L. and Y.D. conceived the ideas, implemented the experimental setup, and designed the experiment. H.L., Y.D., and X.L. designed the NN

structure. X.J. and Y.S. supervised the research and contributed to the ideas.

### Funding

This work was supported by the Natural Science Foundation of China (NSFC) (Grant Nos. 62341508, 62105203) and the Shanghai Municipal Science and Technology Major Project (BH0300071).

### Notes

The authors declare no competing financial interest.

## ACKNOWLEDGMENTS

We thank Professor Weiqiang Xie and Professor Yuye Ling from Shanghai Jiao Tong University for their effective discussions.

## REFERENCES

- (1) Del'Haye, P.; Schliesser, A.; Arcizet, O.; Wilken, T.; Holzwarth, R.; Kippenberg, T. J. Optical Frequency Comb Generation from a Monolithic Microresonator. *Nature* **2007**, *450* (7173), 1214–1217.
- (2) Fortier, T.; Baumann, E. 20 Years of Developments in Optical Frequency Comb Technology and Applications. *Commun. Phys.* **2019**, *2* (1), 153.
- (3) Xu, X.; Tan, M.; Corcoran, B.; Wu, J.; Boes, A.; Nguyen, T. G.; Chu, S. T.; Little, B. E.; Hicks, D. G.; Morandotti, R.; Mitchell, A.; Moss, D. J. 11 TOPS Photonic Convolutional Accelerator for Optical Neural Networks. *Nature* **2021**, *589* (7840), 44–51.
- (4) Newman, Z. L.; Maurice, V.; Drake, T.; Stone, J. R.; Briles, T. C.; Spencer, D. T.; Fredrick, C.; Li, Q.; Westly, D.; Ilic, B. R.; Shen, B.; Suh, M.-G.; Yang, K. Y.; Johnson, C.; Johnson, D. M. S.; Hollberg, L.; Vahala, K. J.; Srinivasan, K.; Diddams, S. A.; Kitching, J.; Papp, S. B.; Hummon, M. T. Architecture for the Photonic Integration of an Optical Atomic Clock. *Optica* **2019**, *6* (5), 680.
- (5) Hu, J.; He, J.; Liu, J.; Raja, A. S.; Karpov, M.; Lukashchuk, A.; Kippenberg, T. J.; Brès, C.-S. Reconfigurable Radiofrequency Filters Based on Versatile Soliton Microcombs. *Nat. Commun.* **2020**, *11* (1), 4377.
- (6) Zhao, Y.; Li, Z.; Ma, X.; Zhou, K.; Guan, W.; Wang, C.; Wu, S.; Liu, H.; Wan, W.; Cao, J. C.; Zhang, Y.; Zeng, H.; Li, H. Stabilized Terahertz Quantum Cascade Laser Dual-Comb Sources with a Hybrid Locking. *ACS Photonics* **2024**, *11* (2), 520–528.
- (7) Xu, X.; Wu, J.; Nguyen, T. G.; Shoeiby, M.; Chu, S. T.; Little, B. E.; Morandotti, R.; Mitchell, A.; Moss, D. J. Advanced RF and Microwave Functions Based on an Integrated Optical Frequency Comb Source. *Opt. Express* **2018**, *26* (3), 2569.
- (8) Feldmann, J.; Youngblood, N.; Karpov, M.; Gehring, H.; Li, X.; Stappers, M.; Le Gallo, M.; Fu, X.; Lukashchuk, A.; Raja, A. S.; Liu, J.; Wright, C. D.; Sebastian, A.; Kippenberg, T. J.; Pernice, W. H. P.; Bhaskaran, H. Parallel Convolutional Processing Using an Integrated Photonic Tensor Core. *Nature* **2021**, *589* (7840), 52–58.
- (9) Zhang, C.; Zhu, Y.; He, B.; Lin, J.; Liu, R.; Xu, Y.; Yi, L.; Zhuge, Q.; Hu, W.; Hu, W.; Chen, Z.; Xie, X. Clone-Comb-Enabled High-Capacity Digital-Analogue Fronthaul with High-Order Modulation Formats. *Nat. Photonics* **2023**, *17* (11), 1000–1008.
- (10) Corcoran, B.; Tan, M.; Xu, X.; Boes, A.; Wu, J.; Nguyen, T. G.; Chu, S. T.; Little, B. E.; Morandotti, R.; Mitchell, A.; Moss, D. J. Ultra-Dense Optical Data Transmission over Standard Fibre with a Single Chip Source. *Nat. Commun.* **2020**, *11* (1), 2568.
- (11) Willits, J. T.; Weiner, A. M.; Cundiff, S. T. Line-by-Line Pulse Shaping with Spectral Resolution below 890 MHz. *Opt. Express* **2012**, *20* (3), 3110.
- (12) Ferdous, F.; Miao, H.; Leaird, D. E.; Srinivasan, K.; Wang, J.; Chen, L.; Varghese, L. T.; Weiner, A. M. Spectral Line-by-Line Pulse Shaping of on-Chip Microresonator Frequency Combs. *Nat. Photonics* **2011**, *5* (12), 770–776.
- (13) Lee, D.; Nakamura, T.; Metcalf, A. J.; Flowers-Jacobs, N. E.; Fox, A. E.; Dresselhaus, P. D.; Quinlan, F. Sub-GHz Resolution Line-

- by-Line Pulse Shaper for Driving Superconducting Circuits. *APL Photonics* **2023**, *8* (8), 086115.
- (14) Lin, G.; Song, Q. Kerr Frequency Comb Interaction with Raman, Brillouin, and Second Order Nonlinear Effects. *Laser Photonics Rev.* **2022**, *16* (1), 2100184.
- (15) Xue, X.; Xuan, Y.; Wang, C.; Wang, P.-H.; Liu, Y.; Niu, B.; Leaird, D. E.; Qi, M.; Weiner, A. M. Thermal Tuning of Kerr Frequency Combs in Silicon Nitride Microring Resonators. *Opt. Express* **2016**, *24* (1), 687.
- (16) Cheng, R.; Yu, M.; Shams-Ansari, A.; Hu, Y.; Reimer, C.; Zhang, M.; Lončar, M. Frequency Comb Generation via Synchronous Pumped  $\chi(3)$  Resonator on Thin-Film Lithium Niobate. *Nat. Commun.* **2024**, *15* (1), 3921.
- (17) Chang, L.; Liu, S.; Bowers, J. E. Integrated Optical Frequency Comb Technologies. *Nat. Photonics* **2022**, *16* (2), 95–108.
- (18) Tan, T.; Peng, C.; Yuan, Z.; Xie, X.; Liu, H.; Xie, Z.; Huang, S.-W.; Rao, Y.; Yao, B. Predicting Kerr Soliton Combs in Micro-resonators via Deep Neural Networks. *J. Light. Technol.* **2020**, *38* (23), 6591–6599.
- (19) Kues, M.; Reimer, C.; Wetzel, B.; Roztocki, P.; Little, B. E.; Chu, S. T.; Hansson, T.; Viktorov, E. A.; Moss, D. J.; Morandotti, R. Passively Mode-Locked Laser with an Ultra-Narrow Spectral Width. *Nat. Photonics* **2017**, *11* (3), 159–162.
- (20) Kim, J.; Song, Y. Ultralow-Noise Mode-Locked Fiber Lasers and Frequency Combs: Principles, Status, and Applications. *Adv. Opt. Photonics* **2016**, *8* (3), 465–540.
- (21) Parriaux, A.; Hammani, K.; Millot, G. Electro-Optic Frequency Combs. *Adv. Opt. Photonics* **2020**, *12* (1), 223.
- (22) Vikram, B. S.; Prakash, R.; Selvaraja, S. K.; Supradeepa, V. R. Enhanced Nonlinear Spectral Broadening and Sub-Picosecond Pulse Generation by Adaptive Spectral Phase Optimization of Electro-Optic Frequency Combs. *Opt. Express* **2020**, *28* (8), 11215.
- (23) Zhuang, R.; Ni, K.; Wu, G.; Hao, T.; Lu, L.; Li, Y.; Zhou, Q. Electro-Optic Frequency Combs: Theory, Characteristics, and Applications. *Laser Photonics Rev.* **2023**, *17* (6), 2200353.
- (24) Stucchi, D.; Corsini, A.; Genty, G.; Boracchi, G.; Foi, A. A Weighted Loss Function to Predict Control Parameters for Supercontinuum Generation Via Neural Networks. In *2021 IEEE 31st International Workshop on Machine Learning for Signal Processing (MLSP)*; IEEE: Gold Coast, Australia, 2021; pp. 1–6.
- (25) Yang, X.; Richardson, D. J.; Petropoulos, P. Nonlinear Generation of Ultra-Flat Broadened Spectrum Based on Adaptive Pulse Shaping. *J. Light. Technol.* **2012**, *30* (12), 1971–1977.
- (26) Wu, J.-L.; Guo, X.; Jiao, Y.; Zhang, X.; Wang, T.; Yang, Y.-D.; Xiao, J.-L.; Zhang, D.; Qin, G.; Huang, Y.-Z. Octave-Spanning Optical Frequency Comb Generation Using a Directly-Modulated Microlaser Source. *J. Light. Technol.* **2022**, *40* (16), 5575–5582.
- (27) Agrawal, G. P. *Nonlinear Fiber Optics*, Sixth Ed.; Academic Press: London, United Kingdom ; San Diego, CA, United States, 2019.
- (28) Hsieh, C.-H.; Li, Y.-S.; Hwang, B.-J.; Hsiao, C.-H. Detection of Atrial Fibrillation Using 1D Convolutional Neural Network. *Sensors* **2020**, *20* (7), 2136.
- (29) Li, X.; Li, J.; An, S.; Liu, H.; Shieh, W.; Su, Y. Deep-Learning-Enabled Direct Detection With Reduced Computational Complexity and High Electrical-Spectral-Efficiency. *J. Light. Technol.* **2023**, *41* (17), 5495–5502.
- (30) Kiranyaz, S.; Avci, O.; Abdeljaber, O.; Ince, T.; Gabbouj, M.; Inman, D. J. 1D Convolutional Neural Networks and Applications: A Survey. *Mech Syst. Signal Process* **2021**, *151*, 107398.
- (31) He, K.; Zhang, X.; Ren, S.; Sun, J. Deep Residual Learning for Image Recognition. In *2016 IEEE Conference on Computer Vision and Pattern Recognition (CVPR)*. IEEE: Las Vegas, NV, USA, 2016; pp. 770–778.
- (32) Yao, C.; Chen, M.; Yan, T.; Ming, L.; Cheng, Q.; Penty, R. Broadband Picometer-Scale Resolution on-Chip Spectrometer with Reconfigurable Photonics. *Light: sci. Appl.* **2023**, *12* (1), 156.
- (33) Yang, T.; Dong, J.; Liao, S.; Huang, D.; Zhang, X. Comparison Analysis of Optical Frequency Comb Generation with Nonlinear Effects in Highly Nonlinear Fibers. *Opt. Express* **2013**, *21* (7), 8508.
- (34) Liao, K.; Dai, T.; Yan, Q.; Hu, X.; Gong, Q. Integrated Photonic Neural Networks: Opportunities and Challenges. *ACS Photonics* **2023**, *10* (7), 2001–2010.